Journal of Molecular Catalysis A: Chemical 308 (2009) 79–86

Contents lists available at ScienceDirect

Journal of Molecular Catalysis A: Chemical

journal homepage: www.elsevier.com/locate/molcata

An excellent Pd-based nanocomposite catalyst for the selective hydrogenation of *para*-chloronitrobenzene

Hongquan Liu, Minghui Liang, Chao Xiao, Ning Zheng, Xuhui Feng, Yan Liu, Jinglin Xie, Yuan Wang*

Beijing National Laboratory for Molecular Sciences, State Key Laboratory for Structural Chemistry of Unstable and Stable Species, College of Chemistry & Molecular Engineering, Peking University, Beijing 100871, PR China

ARTICLE INFO

Article history:
Received 29 January 2009
Received in revised form 17 March 2009
Accepted 20 March 2009
Available online 31 March 2009

Keywords:
Palladium
Nanocomposite catalyst
CO chemisorption
Chloronitrobenzene
Hydrogenation
Hydrodechlorination

ABSTRACT

A partially reduced Pd/γ-Fe_2O_3 nanocomposite catalyst (Pd/γ-Fe_2O_3-PR) was prepared using PdO and ferric hydroxide colloidal particles as starting materials. This catalyst exhibited excellent catalytic properties for the selective hydrogenation of *para*-chloronitrobenzene (*p*-CNB) to *para*-chloroaniline (*p*-CAN). The selectivity to *p*-CAN reached 99.2% at complete conversion of the substrate and intermediates, and the hydrodechlorination of *p*-CAN was fully suppressed over Pd/γ-Fe_2O_3-PR. The byproduct aniline was derived from the hydrodechlorination of *p*-CNB and 4,4′-dichloroazobenzene intermediate, a new hydrodechlorination route. X-ray photoelectron spectroscopy characterization indicated an electron transfer from the partially reduced γ-Fe_2O_3 nanoparticles to the Pd particles in Pd/γ-Fe_2O_3-PR. IR-CO probe and CO chemisorption experimental results revealed that CO could hardly be chemisorbed on the Pd particles in Pd/γ-Fe_2O_3-PR under our experimental conditions, implying an electronic interaction between the Pd particles and γ-Fe_2O_3-PR nanoparticles, which may be a cause of the observed superior selectivity to *p*-CAN over Pd/γ-Fe_2O_3-PR.

1. Introduction

Aromatic chloroamines are important intermediates in the synthesis of dyes, drugs, herbicides, and pesticides [1]. At present these organic amines are generally produced through selective hydrogenation of the corresponding aromatic chloronitro compounds over transition metal catalysts such as noble metals and nickel. In this process the hydrodechlorination of the aromatic chloroamines often occurs over most metal catalysts because of the electron-donating effect of amino groups in the aromatic ring [2]. Recently, Keane and coworkers reported that in the continuous gas phase hydrogenation of *p*-chloronitrobenzene (*p*-CNB) over several supported Ni catalysts, *p*-CAN was produced as a sole product at *p*-CNB conversion of about 15%, which is enlightening for the development of clean routes to produce chloroanilines [3].

Selective hydrogenation of chloronitrobenzenes (CNBs) to the corresponding chloroanilines (CANs) has been intensively studied over Pt and Pt-based alloy catalysts for their high catalytic activities combined with relatively low catalytic hydrodechlorination rates [4–9]. Recently, we reported a magnetic Pt/γ-Fe_2O_3-PR nanocomposite catalyst which was prepared using "unprotected" Pt nanoclusters [10] and ferric hydroxide nanoparticles as building blocks [11]. Over this catalyst, superior selectivities to haloanilines were achieved and hydrodehalogenation of the target haloanilines products was fully suppressed in the hydrogenation of a series of halonitrobenzenes, including *o*-CNB, bromonitrobenzenes (BNBs), 2,4-dinitrochlorobenzene and iodonitrobenzenes [11–13].

Compared with Pt catalysts, Pd catalysts generally exhibit low catalytic selectivity to CANs in the hydrogenation of CNBs because the concomitant hydrodechlorination reactions are serious over usual Pd-based catalysts [14–16]. The most attractive advantage of Pd-based catalysts over Pt-based ones is their low cost. In order to improve the selectivity to CANs in the hydrogenation of CNBs over Pd catalysts, several strategies have been developed, such as introducing some promoting or inhibiting additives to the solution phase [16,17] or to the catalysts [18], alloying Pd with other metals [15,16,19–21], applying partly poisoned catalysts [22–25], conducting the reaction in supercritical carbon dioxide [26] and modulating the metal/support interaction in supported Pd catalysts [1,27]. Generally speaking, introducing soluble additives into the reaction media will increase the difficulty in separating the products. Kralik and coworkers reported that the selectivity to CANs in the hydrogenation of CNBs over a sulphonated poly(styrene-*co*-divinylbenzene) supported Pd catalyst could reach 90% at stoichiometric consumption of hydrogen [1]. Li and coworkers recently markedly improved the *p*-CAN selectivity to 96.6% at *p*-CNB conversion close to 100% over a PVP-Pd/Al_2O_3 catalyst by introducing a soluble salt of Sn^{4+} into the reaction media with a Sn^{4+}/Pd molar ratio of 1:1 [17]. Increasing the dosage of Sn^{4+} further improved the selectivity to *p*-CAN, but decreased the catalytic

* Corresponding author. Tel.: +86 10 6275 7497; fax: +86 10 6276 5769.
E-mail address: wangy@pku.edu.cn (Y. Wang).

1381-1169/$ – see front matter © 2009 Elsevier B.V. All rights reserved.
doi:10.1016/j.molcata.2009.03.033

reaction rate synchronously. Dechlorination reaction was reported to be completely blocked when the molar ratio of Sn^{4+}/Pd was up to 5, while *p*-chloronitrosobenzene (*p*-CNSB) intermediate formed in the reaction was difficult to be totally reduced to *p*-CAN in this condition.

Although intensive efforts have been made to solve the problem of hydrodechlorination in CNB hydrogenation, still it is a challenge to create novel palladium catalysts for further improving the selectivity to CAN at complete conversion of the substrates and intermediates and simultaneously maintaining the high catalytic activity. To the best of our knowledge, the complete suppression of CAN hydrodechlorination over a supported Pd catalyst in the absence of any soluble organic or inorganic additive or modifier has so far been scarce.

In this paper, we report a partially reduced Pd/γ-Fe_2O_3 nanocomposite catalyst (Pd/γ-Fe_2O_3-PR) that exhibited high catalytic activity and superior selectivity to *p*-CAN in the hydrogenation of *p*-CNB. The hydrodechlorination of *p*-CAN was fully suppressed at complete conversion of *p*-CNB and other intermediates and the selectivity to *p*-CAN reached 99.2% at 303 K and 4 MPa. A hydrodechlorination route over Pd/γ-Fe_2O_3-PR, i.e. through the hydrodechlorination of 4,4′-dichloroazobenzene intermediate was revealed for the first time. The ferromagnetic Pd/γ-Fe_2O_3-PR nanocomposite catalyst could be conveniently separated from the reaction system in an applied magnetic field and exhibited good reusability.

X-ray photoelectron spectroscopy (XPS) measurements revealed an electron transfer from the partially reduced γ-Fe_2O_3 particles to the Pd particles in Pd/γ-Fe_2O_3-PR. Moreover, it was found for the first time that CO could hardly be chemisorbed on the Pd particles deposited on the partially reduced γ-Fe_2O_3 nanoparticles under our measurement conditions. We believe that these characteristics are important causes of the superior selectivity to *p*-CAN in the hydrogenation of *p*-CNB over Pd/γ-Fe_2O_3-PR.

2. Experimental

2.1. Reagents

Hydrogen (99.999%) was supplied by Beijing Gases Company. Pd/C (Pd: 3 wt%) was purchased from Acros. Methanol (HPLC grade, 99.9%) was purchased from Fisher. Other reagents used in this work were of analytical grade.

2.2. Catalyst preparation

2.2.1. Colloid preparation

A dark-red hydrosol of PdO was prepared simply by adding an aqueous solution of sodium hydroxide (0.2 M) to a solution of $PdCl_2$ (2.82×10^{-2} mol/L) in 20 ml water to adjust pH to 12. The colloid solution of ferric hydroxide was prepared according to a method reported previously [11]. An aqueous solution of ammonia (10%) was added to a solution of $FeCl_3$ (4%) in 100 ml of water to adjust pH to about 7.5, producing a precipitate that was separated by a filter, washed with water, and peptized in 60 ml of aqueous solution of $FeCl_3$ (1%), resulting in a transparent colloidal solution of ferric hydroxide.

2.2.2. Catalyst preparation

The Pd/γ-Fe_2O_3 nanocomposite catalyst was prepared as follows: 30 ml of the prepared hydrosol of PdO was mixed with 60 ml of ferric hydroxide colloidal solution at required ratio under stirring to obtain a complex sol. After stirring for 0.5 h, 90 ml of ethylene glycol was added to the complex sol. The mixture was then refluxed under a N_2 flow for 2 h, and then a solution of sodium glycollate (0.5 g in 1 ml water) was added to the reaction system. The obtained mixture was further refluxed for 20 h to produce a magnetic precipitate which was separated by an applied magnetic field, washed with water, and dried at 353 K in air, producing a brownish-red solid of Pd/γ-Fe_2O_3. The Pd content of the prepared catalyst was measured to be 3.0 wt% by inductively coupled plasma-atomic emission spectroscopy (ICP-AES, PROFILE SPEC, LEEMAN LABS).

2.3. Catalytic hydrogenation of p-CNB

Hydrogenation of *p*-CNB was carried out in a 50-ml reactor with magnetic stirring at 303 K and atmospheric pressure of H_2. Prior to the reaction, air in the system was replaced by hydrogen 20 times, and the catalyst, Pd/γ-Fe_2O_3 (3 wt%, 15.0 ± 0.1 mg) or Pd/C (3 wt%, 5.0 ± 0.1 mg), dispersed in 10 ml methanol, was activated under hydrogen for 180 min. Then a methanol solution of *p*-CNB was added to the reactor to start the reaction. The hydrogen uptake was monitored by a constant pressure gas burette. The products were identified by GC–MS coupling (Perkin-XL) and quantitatively analyzed by gas chromatography (Shimadzu GC-2010), using a flame ionization detector and a capillary column Rtx-5 MS (Ø0.25 mm × 60 m). Biphenyl as an internal standard substance was added into the samples for GC measurement rather than into the reaction system, to avoid its influence on the reaction. The semi-quantitative analysis of trace aniline (AN) in the reaction mixture was also conducted by comparing the AN peak area in GC with those of standard solutions with ratios of AN to *p*-CAN less than 0.7%. Different amounts of the catalysts were used in the hydrogenation reaction in order to avoid the diffusion control on the reaction rate.

2.4. Characterization of the catalyst

2.4.1. IR-CO probe characterization of the catalysts

In a typical experiment, the Pd/γ-Fe_2O_3 (25 mg) catalyst was ground under air and pressed into a self-supporting wafer with a diameter of 1.5 cm, which was treated in the IR cell under vacuum of $1–3 \times 10^{-5}$ Torr at 373 K for 2 h to remove adsorbed water and impurities on the sample. After the sample was cooled to 303 K, 5 kPa of CO was charged into the IR cell to achieve the chemisorption equilibrium. The gaseous CO was removed by evacuation, and the spectrum of CO adsorbed on the catalyst was recorded on a FTIR spectrometer (Tensor 27, Bruker) with a resolution of 4 cm^{-1}. The IR spectrum of the sample before exposure to CO was used as a subtraction background.

In another experiment, a self-supporting wafer of the Pd/γ-Fe_2O_3 catalyst (25 mg) was first treated under flowing hydrogen at 308 K for 5 h to form a partially reduced Pd/γ-Fe_2O_3 catalyst (Pd/γ-Fe_2O_3-PR) that was then heated at 573 K in vacuum for 3 h in the IR cell. IR-CO probe measurements on this sample were conducted in the same manner and conditions as applied in the typical experiment.

2.4.2. CO chemisorption on the catalysts

In the chemisorption experiments on the Pd/γ-Fe_2O_3-PR and fresh Pd/γ-Fe_2O_3 catalysts, the CO/Pd ratio was determined on Micromeritics ASAP 2010C instrument. In the analysis of the Pd/γ-Fe_2O_3-PR, 0.05 g of Pd/γ-Fe_2O_3 (Pd: 3 wt%) was loaded into a U-type tube and treated in the following steps: evacuation at 308 K for 0.5 h and then at 473 K for 1 h, reduction by flowing hydrogen at 308 K for 3 h, and evacuation at 573 K for 2 h and at 308 K for 0.5 h. The CO adsorption was measured at 308 K and at 4–50 kPa of CO. The fresh Pd/γ-Fe_2O_3 catalyst was treated and analyzed as described previously, except for the hydrogen reduction process.

2.4.3. XPS measurement of the catalysts

XPS measurements were carried out with an Axis Ultra photoelectron spectrometer using an AlKα (1486.7 eV) X-ray source,

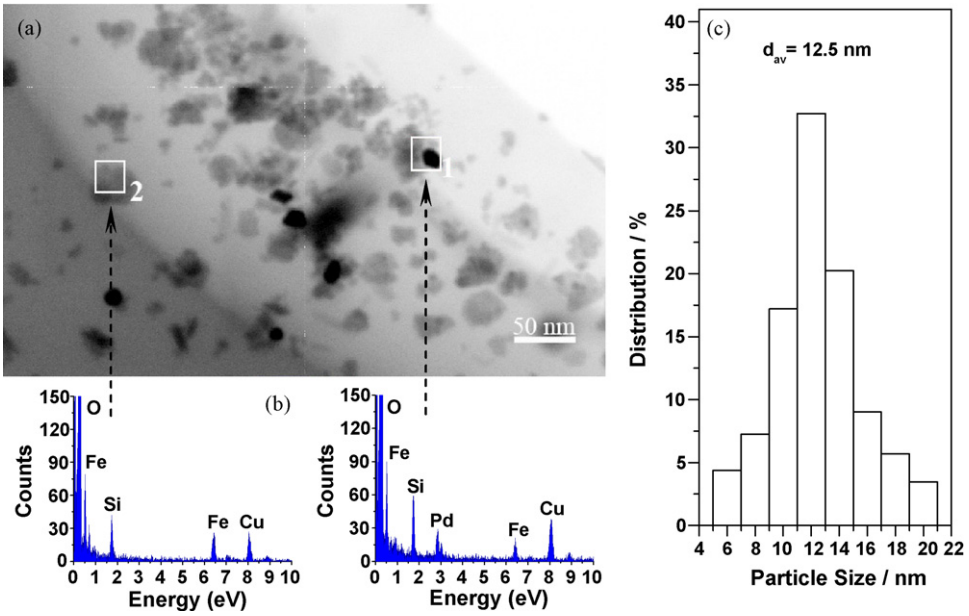

Fig. 1. STEM image (a), area-selected EDX spectra (b) of Pd/γ-Fe_2O_3, and the size distribution of Pd particles in Pd/γ-Fe_2O_3 (c).

with the pressure of the measuring chamber set at 5×10^{-9} Torr. The binding energy scales for the samples were referenced by setting the C 1s binding energy of contamination carbon to 284.8 eV. The Pd/γ-Fe_2O_3-PR catalyst for the XPS measurement was prepared by reducing fresh Pd/γ-Fe_2O_3 (Pd: 3 wt%) with hydrogen at 308 K for 5 h in the pretreatment chamber of the XPS spectrometer. The sample was moved to the analysis chamber after the pretreatment chamber was flushed with argon and evacuated. For comparison, Pd powder was also treated with hydrogen and then analyzed in the same manner and conditions.

2.4.4. STEM, XRD and BET characterization of the catalysts

STEM images were taken on a Philips Tecnai F30 scanning transmission electron microscope equipped with a high-angle-annular dark-field (HAADF) detector. The sample was prepared by dispersing Pd/γ-Fe_2O_3 in 10 ml of water solution containing 10 mg polyvinylpyrrolidone (PVP) followed by ultrasound irradiation for several minutes. A drop of the dilute suspension was placed onto a copper grid covered with a carbon film. Excess liquid was removed by a piece of filter paper. The sample was dried in vacuum at room temperature for 12 h. The particle size distribution histogram was obtained on the basis of the measurements of 250 particles. The XRD patterns were recorded on a Rigaku D/max 2500 diffractometer operated at 40 kV voltage and 300 mA current with a Cu radiation source. The specific surface area of the catalyst was measured on a Micromeritics ASAP 2010M instrument.

3. Results and discussion

Fig. 1a shows the STEM image of the Pd/γ-Fe_2O_3 nanocomposite catalyst. Combined EDX analysis (Fig. 1b) revealed that black spots in Fig. 1a are the image of palladium nanoparticles which locate on the surfaces of Fe_2O_3 nanoparticles (the grey area in the photograph). The Pd particles in the Pd/γ-Fe_2O_3 catalyst have an average diameter of 12.5 nm, with a size distribution from 5 to 21 nm (Fig. 1c).

Fig. 2a illustrates the XRD pattern of the fresh Pd/γ-Fe_2O_3 (Pd: 3 wt%) nanocomposite catalyst. Diffraction peaks with $2\theta = 30.2^\circ$, 35.7°, 43.4°, 57.4°, 63.0°, are the signals of maghemite nanoparticles in the Pd/γ-Fe_2O_3 catalyst [28]. The diffraction peaks at $2\theta = 40.1^\circ$, 46.6° and 68.1° are the characteristic signals of the face centered cubic crystalline phase of Pd. The average crystal size of Pd in the Pd/γ-Fe_2O_3 nanocomposite is 13.4 nm as calculated from the (1 1 1) diffraction peak using the Scherrer formula, which is consistent with the results of TEM analysis. When Pd/γ-Fe_2O_3 catalyst was activated with hydrogen at 303 K and atmosphere pressure, a color change from brownish-red to black was observed. The XRD pattern of the activated Pd/γ-Fe_2O_3 catalyst is shown in Fig. 2b. The sample for this measurement was prepared by treating Pd/γ-Fe_2O_3 in methanol with hydrogen for 5 h at 303 K. Then it was separated by an applied magnetic field and dried in vacuum at room temperature. It can be discerned that several diffraction peaks slightly shift to the lower angle side relative to those in the fresh Pd/γ-Fe_2O_3 catalyst (see the insert of Fig. 2). Thus we can speculate that Pd/γ-Fe_2O_3 was partially reduced in the activation process, catalyzed by the Pd particles, which was similar to the phenomenon that we

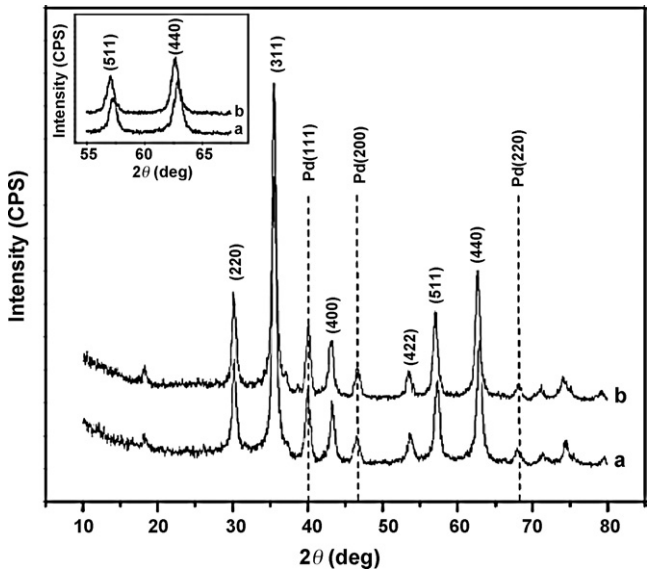

Fig. 2. XRD pattern of the fresh Pd/γ-Fe_2O_3 nanocomposite catalyst (a) and the catalyst activated with hydrogen at 308 K and atmospheric pressure (b). The insert shows the shift of the diffraction peaks of the activated Pd/γ-Fe_2O_3 catalyst.

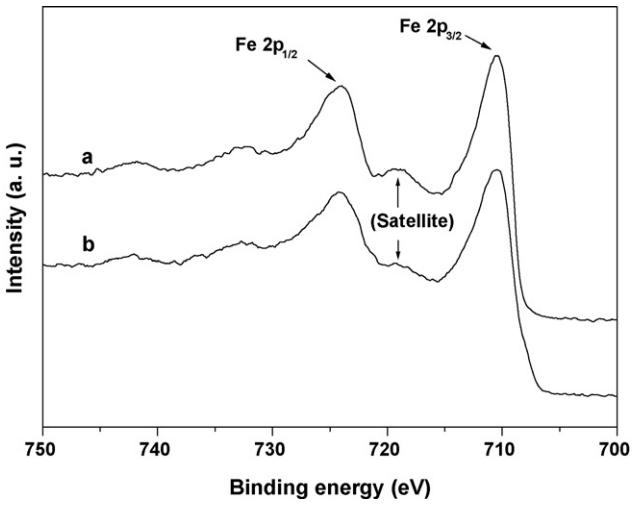

Fig. 3. The core-level spectra of Fe 2p in Pd/γ-Fe_2O_3 (a) and Pd/γ-Fe_2O_3-PR (b). The binding energy scales for these samples were referenced by setting the C 1s binding energy of contamination carbon to 284.8 eV.

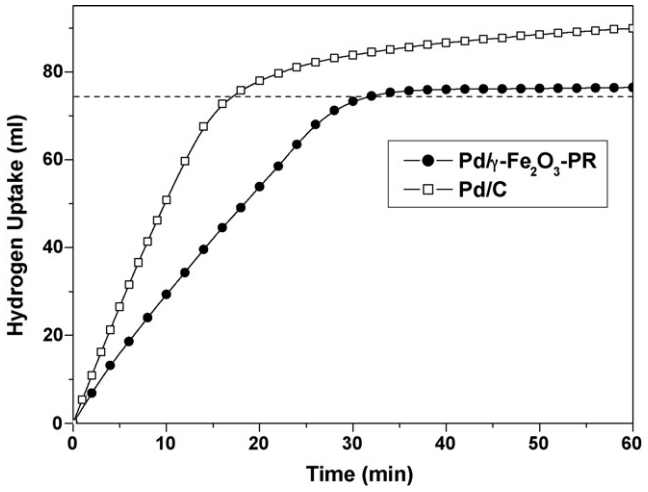

Fig. 4. Cumulative hydrogen uptake of *p*-CNB hydrogenation over Pd/C and Pd/γ-Fe_2O_3-PR catalysts. Reaction conditions: temperature, 303 K; hydrogen pressure, 0.1 MPa; substrate, 1 mmol; solvent, 20 ml methanol; Pd in catalyst, 4.23×10^{-3} mmol for Pd/γ-Fe_2O_3-PR, 1.41×10^{-3} mmol for Pd/C.

previously observed over the Pt/γ-Fe_2O_3 catalyst [12]. The partially reduced Pd/γ-Fe_2O_3 catalyst was designated as Pd/γ-Fe_2O_3-PR.

The partial reduction state of the Fe_2O_3 particles in activated Pd/γ-Fe_2O_3 was further confirmed by XPS measurements. The XPS spectra of Fe 2p in Pd/γ-Fe_2O_3 and Pd/γ-Fe_2O_3-PR catalysts are shown in Fig. 3. The satellite peak near 719 eV as a characteristic of γ-Fe_2O_3, which does not appear in the XPS spectrum of Fe_3O_4 [29], can be clearly seen in the spectrum of Pd/γ-Fe_2O_3 (Fig. 3a). The intensity of this satellite peak decreased obviously after the sample was treated with hydrogen at 308 K for 5 h (Fig. 3b), confirming that γ-Fe_2O_3 particles in Pd/γ-Fe_2O_3 had been partially reduced during the activation process.

Fig. 4 shows the cumulative hydrogen uptake curves in the hydrogenation of *p*-CNB over Pd/γ-Fe_2O_3-PR and a Pd/C catalyst. Over Pd/γ-Fe_2O_3-PR, hydrogen consumption increased almost linearly within 25 min followed by a slow increase of hydrogen uptake. After 40 min, no more increase in the hydrogen uptake was detected with the extension of reaction time. The recorded amount of hydrogen uptake was only slightly larger than the theoretic amount for the complete transformation of *p*-CNB into *p*-CAN. A quite different hydrogen uptake curve was observed over the Pd/C catalyst, which was characterized by a fast initial rate of hydrogen consumption, with a durative and obvious increase in hydrogen uptake after the stoichiometric hydrogen consumption for producing *p*-CAN. In this measurement, 5 mg of Pd/C was used to avoid any significant mass diffusion limitation on the reaction rate.

Table 1 lists the catalytic properties for the hydrogenation of *p*-CNB over the Pd/C and Pd/γ-Fe_2O_3-PR catalysts. The Pd/C catalyst was a very active catalyst in this reaction, with an initial hydrogenation uptake rate of 2.5 $mol_{hydrogen}/(mol_{Pd}\ s)$ at 303 K and 0.1 MPa. However, the selectivity to the desired product *p*-CAN over this catalyst was poor. The yields of *p*-CAN and AN were 50.7% and 49.0%, respectively, when the reaction completed (defined as the complete conversion of the substrate and all intermediates). When the reaction time was extended to 60 min, the yield of the desired product *p*-CAN decreased to 22.1% and the yield of AN increased to 77.4%. At 303 K and 0.1 MPa, the initial hydrogenation uptake rate in the hydrogenation of *p*-CNB over Pd/γ-Fe_2O_3-PR (4.9×10^{-1} $mol_{hydrogen}/(mol_{Pd}\ s)$) was 19.6% of that over the Pd/C catalyst. This is partly due to the fact that Pd particles (d_{av} = 12.5 nm) in Pd/γ-Fe_2O_3-PR are much larger than that in the Pd/C catalyst (d_{av} = 3.0 nm) with a size distribution from 1 to 6 nm as revealed by TEM analysis. Superior selectivity to *p*-CAN was achieved over Pd/γ-Fe_2O_3-PR in this hydrogenation reaction. At 303 K and 0.1 MPa, the selectivity to *p*-CAN reached to 96.2% when the reaction was complete at 41 min, and the content of AN in the final products was only 3.6%. Extending the reaction time to 300 min, no increase in the content of the dechlorination byproduct was detected, suggesting that the hydrodechlorination of *p*-CAN was fully suppressed over the Pd/γ-Fe_2O_3-PR catalyst. The effects of hydrogen pressure and the concentration of substrate on the reaction rate and selectivity to *p*-CAN were investigated in the hydrogenation of *p*-CNB over Pd/γ-Fe_2O_3-PR. As listed in Table 2, when the H_2 pressure was elevated from 0.1 to 4 MPa, the average formation rate of *p*-CAN increased by 3.2 times, and the selectivity to *p*-CAN was improved from 96.2% to 98.6%. Moreover, the average *p*-CAN formation rate was accelerated to 8.6×10^{-1} $mol_{p\text{-}CAN}/(mol_{Pd}\ s)$ and the selectivity to *p*-CAN was improved to 99.2% when the reaction was conducted at 4 MPa

Table 1
Catalytic properties of Pd/γ-Fe_2O_3-PR and Pd/C for the hydrogenation of *p*-CNB[a].

Catalyst	Pd in catalyst (mmol)	Reaction time (min)	Initial H_2 uptake rate[b]	Yield of products (mol%)		
				p-CAN	AN	Others[c]
Pd/C	1.41×10^{-3}	26[d]	2.5	50.7 ± 0.2	49.0 ± 0.2	<0.3
Pd/C	1.41×10^{-3}	60		22.1 ± 0.2	77.4 ± 0.2	<0.5
Pd/γ-Fe_2O_3-PR	4.23×10^{-3}	41[d]	4.9×10^{-1}	96.2 ± 0.2	3.6 ± 0.2	<0.2
Pd/γ-Fe_2O_3-PR	4.23×10^{-3}	300		96.1 ± 0.2	3.6 ± 0.2	<0.3

[a] Reaction conditions: temperature, 303 K; hydrogen pressure, 0.1 MPa; substrate, 1 mmol; solvent, 20 ml methanol.
[b] $mol_{hydrogen}/(mol_{Pd}\ s)$; the uncertainty of the initial H_2 uptake rate was less than 5%.
[c] Over Pd/γ-Fe_2O_3-PR a main byproduct was characterized to be *p*-$ClC_6H_4N{=}CH_2$, which was derived from the condensation of HCHO and *p*-CAN. HCHO was produced from the oxidation of MeOH due to the existence of a trace amount of oxygen in this reaction system in the initial stage of the experiments.
[d] Reaction time for the complete conversion of the substrate and all intermediates.

Table 2
Effects of reaction hydrogen pressure and substrate concentration on the hydrogenation of *p*-CNB over Pd/γ-Fe_2O_3-PR[a].

Catalyst	*p*-CNB (mmol)	H_2 pressure (MPa)	Reaction time (min)	Reaction rate[b]	Yield of products (mol%)		
					p-CAN	AN	Others
Pd/γ-Fe_2O_3-PR	1.0	0.1	41	9.2×10^{-2}	96.2 ± 0.2	3.6 ± 0.2	<0.2
Pd/γ-Fe_2O_3-PR	1.0	1.0	23	1.7×10^{-1}	98.3 ± 0.2	1.4 ± 0.2	<0.3
Pd/γ-Fe_2O_3-PR	1.0	2.0	12	3.2×10^{-1}	98.4 ± 0.2	1.3 ± 0.2	<0.3
Pd/γ-Fe_2O_3-PR	1.0	4.0	10	3.9×10^{-1}	98.6 ± 0.2	1.2 ± 0.2	<0.2
Pd/γ-Fe_2O_3-PR	1.0	4.0	300	–	98.5 ± 0.2	1.2 ± 0.2	<0.3
Pd/γ-Fe_2O_3-PR	20.9	4.0	95	8.6×10^{-1}	99.2 ± 0.2	<0.7	<0.1
Pd/γ-Fe_2O_3-PR	20.9	4.0	300	–	99.2 ± 0.2	<0.7	<0.1

[a] Reaction conditions: temperature, 303 K; solvent, 20 ml methanol; Pd in catalyst, 4.23×10^{-3} mmol.
[b] Average formation rate of *p*-CAN ($mol_{p\text{-CAN}}/(mol_{Pd}\ s)$); the uncertainty was less than 5%.

with a *p*-CNB concentration of about 1 mol/L. The selectivity to *p*-CAN could also be maintained with the extension of reaction time after the reaction completed even at such conditions.

For comparison, we measured the catalytic properties at 303 K and 0.1 MPa for the reaction of interest over the previously reported Pt/γ-Fe_2O_3-PR nanocomposite catalyst which had an average diameter of Pt particles of 2.2 nm [13]. Over Pt/γ-Fe_2O_3-PR, the average formation rate and the selectivity of *p*-CAN were measured to be 8.2×10^{-2} $mol_{p\text{-CAN}}/(mol_{Pt}\ s)$ and 99.9%, respectively. These results suggest that Pd/γ-Fe_2O_3-PR is more active than Pt/γ-Fe_2O_3-PR as a catalyst for the selective hydrogenation of *p*-CNB under given conditions (see Table 2).

To testify the suppression function of γ-Fe_2O_3-PR particles in Pd/γ-Fe_2O_3-PR for *p*-CAN dechlorination, we compared the catalytic hydrogenolysis reaction of *p*-CAN over the Pd/C, Pd/γ-Fe_2O_3-PR and Pd/γ-Fe_2O_3 catalysts. As shown in Table 3, the Pd/C catalyst exhibited high catalytic activity for the hydrodechlorination of *p*-CAN. When the hydrogenolysis of *p*-CAN was conducted for 60 min, the yield of AN reached 73.2% and only 26.8% of *p*-CAN remained. Over Pd/γ-Fe_2O_3-PR, however, no AN was detected during the reaction process of 300 min, further confirming that the hydrodechlorination of *p*-CAN was fully suppressed over this catalyst. Over the fresh Pd/γ-Fe_2O_3 catalyst without activation under H_2 before the reaction, dechlorination of *p*-CAN occurred at the initial stage of the reaction. With the extension of reaction time, the fresh Pd/γ-Fe_2O_3 catalyst transformed into a partially reduced catalyst, accompanied with a color change from brownish-red to black, and the dechlorination reaction was suppressed finally. This phenomenon indicated that the partial reduction of fresh Pd/γ-Fe_2O_3 in the activation process prior to the reaction is utmost important to completely suppress the hydrodechlorination of *p*-CAN.

Scheme 1 depicts the widely accepted reaction routes for the hydrogenation of CNBs [2,30]. It can be seen that there are two main routes for CANs (**4**) formation. One (**I**) is the direct reduction of nitro groups in CNBs (**1**), through the nitroso- (**2**) and hydroxylamino- (**3**) intermediates to CAN products; the other (**II**) is the condensa-

Table 3
Hydrodechlorination of *p*-CAN over Pd/C, Pd/γ-Fe_2O_3-PR and Pd/γ-Fe_2O_3[a].

Catalyst	Pd in catalyst (mmol)	Reaction time (min)	Composition (mol%)		Dechlorination rate[b]
			p-CAN	AN	
Pd/C	1.41×10^{-3}	60	26.8 ± 0.2	73.2 ± 0.2	1.4×10^{-1}
Pd/γ-Fe_2O_3-PR[c]	4.23×10^{-3}	300	>99.9	<0.1	–
Pd/γ-Fe_2O_3[d]	4.23×10^{-3}	60	98.5 ± 0.2	1.5 ± 0.2	9.9×10^{-4}
Pd/γ-Fe_2O_3[d]	4.23×10^{-3}	180	98.4 ± 0.2	1.6 ± 0.2	–
Pd/γ-Fe_2O_3[d]	4.23×10^{-3}	300	98.4 ± 0.2	1.6 ± 0.2	–

[a] Reaction conditions: temperature, 303 K; hydrogen pressure, 0.1 MPa; substrate, 1 mmol; solvent, 20 ml methanol.
[b] Average rate of *p*-CAN dechlorination ($mol_{p\text{-CAN}}/(mol_{Pd}\ s)$); the uncertainty was less than 5%.
[c] Catalyst was activated at 303 K and 0.1 MPa of hydrogen pressure for 180 min before used for the reaction.
[d] Catalyst was used without the activation process.

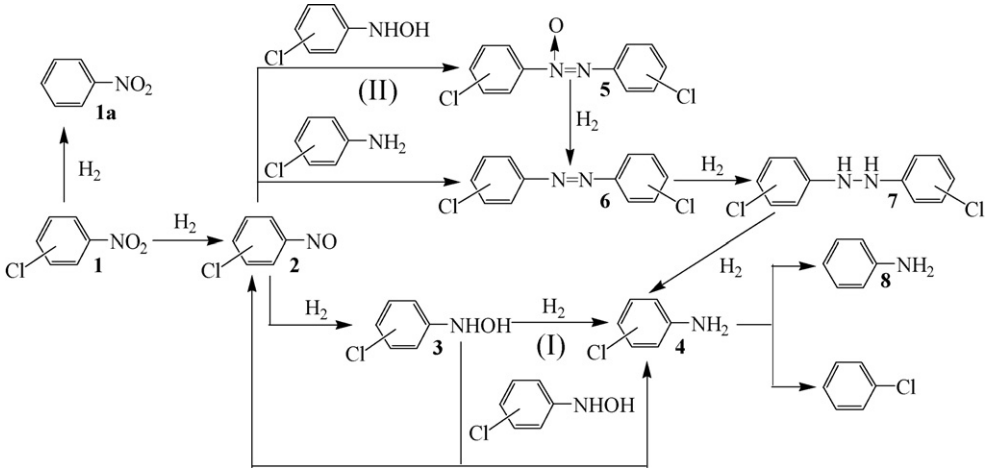

Scheme 1. The widely accepted reaction routes of hydrogenation of CNBs.

tion of nitroso- (**2**) and hydroxylamino- (**3**) intermediates to form dimeric intermediates of dichloroazoxybenzenes (**5**), followed by the hydrogenation of them to azo- (**6**) and hydrazo- (**7**) intermediates and finally to CAN products. It is known that dechlorination reaction can occur on CNBs and CANs to form nitrobenzene (**1a**) and aniline (**8**), respectively, over most Pd catalysts.

For the hydrogenation of *p*-CNB over the present Pd/γ-Fe_2O_3-PR nanocomposite catalyst, we analyzed the reaction species at different time during the reaction process by GC and GC–MS. A series of reaction compounds, including *p*-CNB (**1**), the products of *p*-CAN (**4**) and AN (**8**), *p*-CNSB (**2**) and 4,4′-dichloroazoxybenzene (**5**) intermediates as well as a trace of nitrobenzene (NB) (**1a**) were detected during the reaction process. The evolution of *p*-CNB, *p*-CAN and AN along with time is shown in Fig. 5a. The appearance, increase, decrease and finally disappearance of *p*-CNSB, 4,4′-dichloroazoxybenzene and NB in this reaction are depicted in Fig. 5b. These results indicated that the hydrogenation of *p*-CNB over Pd/γ-Fe_2O_3-PR occurred through the routes (**I**) and (**II**) simultaneously. Meanwhile, the appearance of NB verified the hydrodechlorination of *p*-CNB over our Pd/γ-Fe_2O_3-PR catalyst.

The hydrodechlorination of *p*-CNB may be not the only pathway to produce AN over Pd/γ-Fe_2O_3-PR because other hydrodechlorination routes such as the hydrodechlorination of reaction intermediates cannot be ruled out. Recently, we revealed a hydrodebromination pathway for the first time in the hydrogenation of BNBs over a Pt/γ-Fe_2O_3-PR nanocomposite catalyst, i.e. through the hydrodebromination of the condensed intermediates [12]. Hydrodehalogenation of condensed intermediates was scarcely reported perhaps due to the difficulty in distinguishing the hydrodehalogenation of these intermediates from that of haloanilines over most catalysts. In the present work, the excellent properties of Pd/γ-Fe_2O_3-PR nanocomposite catalyst allow us to further ascertain this dehalogenation pathway. Hydrogenation of 4,4′-dichloroazoxybenzene (synthesized according to the literature [31]) was investigated over Pd/γ-Fe_2O_3-PR and the evolution of reaction species at different time was monitored by GC and GC–MS. As a result, 4,4′-dichloroazobenzene (**5**), *p*-CAN (**4**), the dechlorination byproducts of 4-chloroazobenzene (**9**) and AN (**8**) were detected. Since 4-chloroazoxybenzene was not detected in this reaction, it could be deduced that the hydrodechlorination of 4,4′-dichloroazobenzene produced 4-chloroazobenzene which entered further reactions resulting in 4-chlorohydrazobenzene (**10**) and AN. According to the present experimental results, we proposed the hydrodechlorination pathways in the hydrogenation of *p*-CNB over Pd/γ-Fe_2O_3-PR as shown in Scheme 2.

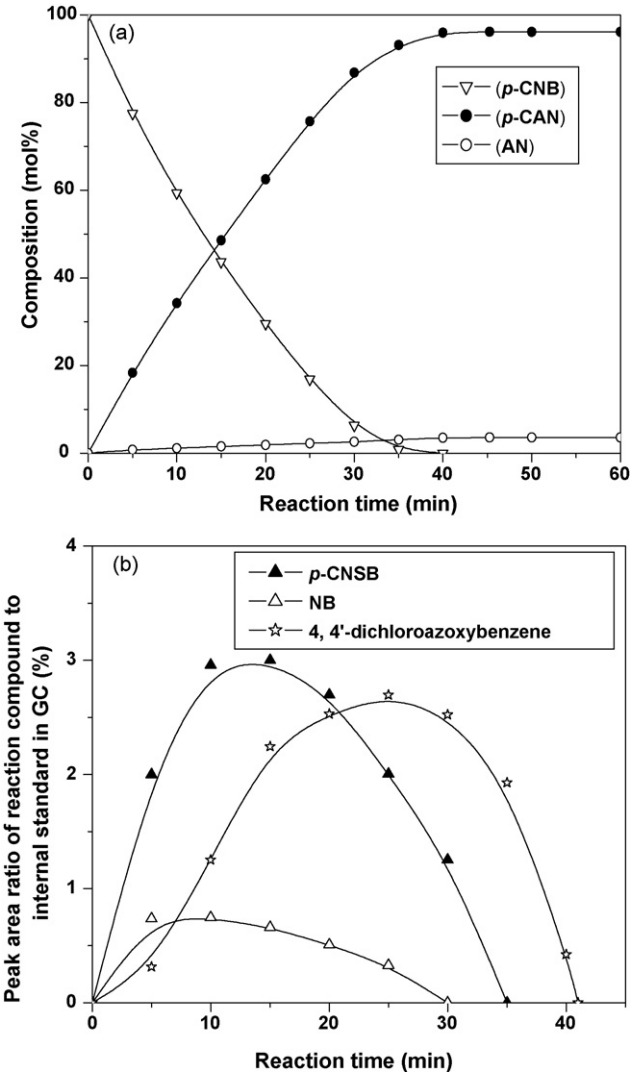

Fig. 5. Evolution of the reaction mixture as a function of time in the hydrogenation of *p*-CNB over Pd/γ-Fe_2O_3-PR. (a) Evolution of *p*-CNB, *p*-CAN and AN; (b) evolution of *p*-CNSB, 4,4′-dichloroazoxybenzene and NB. Reaction conditions were similar to those in Fig. 4.

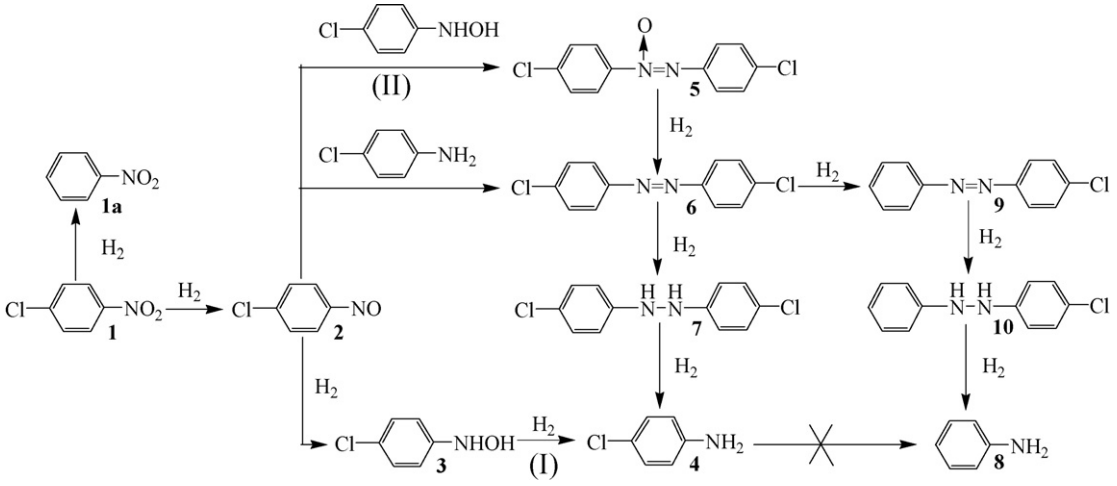

Scheme 2. Reaction pathways for the hydrogenation of *p*-CNB over Pd/γ-Fe_2O_3-PR.

Table 4
Reusability of Pd/γ-Fe_2O_3-PR in the hydrogenation of *p*-CNB[a].

Time reused	Reaction time (min)[b]	Yield of products (mol%)		
		p-CAN	AN	Others
1	41	96.1 ± 0.2	3.6 ± 0.2	<0.3
2	42	96.9 ± 0.2	2.9 ± 0.2	<0.2
3	43	97.2 ± 0.2	2.6 ± 0.2	<0.2
4	48	97.2 ± 0.2	2.5 ± 0.2	<0.3
5	54	97.2 ± 0.2	2.4 ± 0.2	<0.4

[a] Reaction conditions are similar to those in Table 2.
[b] Reaction time for the complete conversion of the substrate and all intermediates.

To explore the stability of Pd/γ-Fe_2O_3-PR, the catalyst was separated from the reaction system by an applied magnetic field after the *p*-CNB hydrogenation reaction completed, washed with methanol and reused in a new reaction cycle. As listed in Table 4, reaction time for the complete conversion of the substrate and intermediates prolonged 32% in the fifth cycle compared to that in the first cycle. Study on the deactivation mechanism of the catalyst in this reaction is going on in our laboratory. In view of the mechanical loss of the catalyst in these experiments, the stability of Pd/γ-Fe_2O_3-PR in the reaction of interest is acceptable for real applications. From Table 4 it can also be seen that the high selectivity to *p*-CAN was maintained over the recycled catalyst.

In the hydrogenation of CNBs over usual Pd catalysts, hydrodechlorination occurs on both the substrates and CANs [2,32], and it may also occur on the condensed intermediates. However, over Pd/γ-Fe_2O_3-PR, hydrodechlorination occurred only on the *p*-CNB and 4,4′-dichloroazobenzene intermediate, but not on *p*-CAN product. This could be attributed to the specific interaction between the partially reduced iron oxide and Pd particles in Pd/γ-Fe_2O_3-PR.

To investigate this peculiar metal/support interaction, we conducted XPS measurements on the Pd/γ-Fe_2O_3-PR catalyst. Pd metal powder was also measured in the same condition for comparison. The Pd metal powder was prepared by adding an equal volume of ethylene glycol to the hydrosol of PdO and then refluxing the mixture at 403 K for 3 h under a N_2 flow. The produced Pd precipitate was washed with methanol and water for several times until no Cl^- was found by $AgNO_3$ detection, dried under vacuum at room temperature and finally reduced in H_2 at 473 K for 1 h. The binding energy of the Pd $3d_{5/2}$ core-level in Pd/γ-Fe_2O_3-PR has a value of 334.8 eV, 0.5 eV lower than that of the Pd power (335.3 eV). This indicated an electron transfer from the partially reduced γ-Fe_2O_3 particles to the Pd particles in Pd/γ-Fe_2O_3-PR.

IR-CO probe and CO chemisorption experiments were conducted on Pd/γ-Fe_2O_3 and Pd/γ-Fe_2O_3-PR for further exploring the metal/support interaction in these catalysts. Fig. 6a shows the IR spectrum of CO adsorbed on the fresh Pd/γ-Fe_2O_3 catalyst. In this spectrum, a broad band in the range of 1830–1980 cm^{-1} can be ascribed to the signals of bridge and threefold bonded CO on the surfaces of Pd particles, while a weak peak centered at 2060 cm^{-1} is the signal of CO adsorbed on the on-top sites of Pd particles' surfaces [33–36]. However, these typical signals of CO adsorbed on Pd were not detected in our IR-CO probe measurements on Pd/γ-Fe_2O_3-PR (Fig. 6b). To confirm the weak chemisorption of CO on Pd/γ-Fe_2O_3-PR, we measured the amounts of CO chemisorbed on the Pd particles in the Pd/γ-Fe_2O_3 and Pd/γ-Fe_2O_3-PR catalysts. For the fresh Pd/γ-Fe_2O_3 catalyst, the CO/Pd ratio in the CO chemisorption experiment was determined to be 15% (Fig. S1). In contrast, the measured CO/Pd ratio was close to zero (Fig. S2) for the partially reduced catalyst Pd/γ-Fe_2O_3-PR treated under the same conditions, which further consolidated the finding of weak CO chemisorption on the surfaces of Pd particles in Pd/γ-Fe_2O_3-PR. In our previous work [13], we have clearly revealed that the partially reduced Pt/γ-Fe_2O_3 catalyst could hardly chemisorb CO under the given experimental conditions and exhibited superior selectivity to haloanilines in the hydrogenation reaction of halonitrobenzenes, which is quite similar to the properties of Pd/γ-Fe_2O_3-PR.

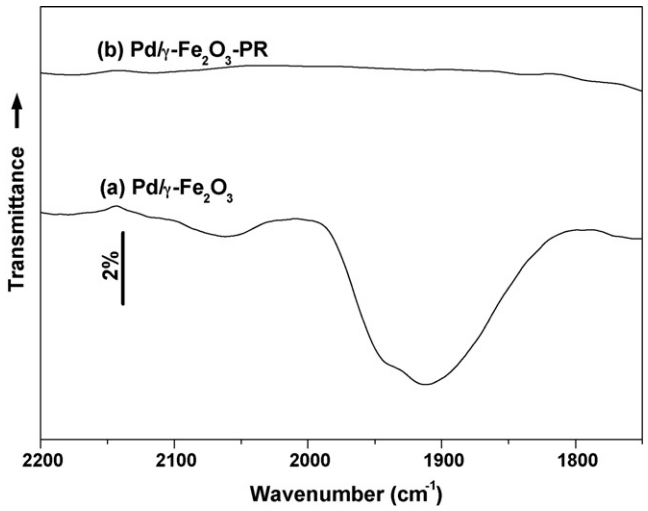

Fig. 6. Infrared spectra of CO chemisorbed on fresh Pd/γ-Fe_2O_3 (a) and Pd/γ-Fe_2O_3-PR (b).

An intrinsic relationship between the CO adsorption characteristic and the hydrodechlorination activity over the Pd/γ-Fe_2O_3-PR catalyst can be inferred. Generally speaking, CO chemically adsorbed on Pd acts as a Lewis base by sharing its electrons in carbon atom with Pd [35,37]. Electron transfer from other species to Pd may lead to a stronger Pauli repulsion with CO and result in a weak Pd–CO interaction [38]. Substituted chlorobenzenes such as *p*-CAN adsorbed on Pd can share their electrons of chlorine atoms with Pd and weaken the carbon–chlorine bond in the adsorbed molecules [39], which may increase the susceptibility of *p*-CAN to hydrodechlorination. Therefore, it is reasonable to speculate that the activation of C–Cl bond in *p*-CAN over Pd/γ-Fe_2O_3-PR is weak because the CO chemisorption on the Pd particles in Pd/γ-Fe_2O_3-PR is too weak to be detected in our experiments. This should be a cause of the high selectivity to *p*-CAN in the hydrogenation of *p*-CNB over Pd/γ-Fe_2O_3-PR. In view of the electron transfer from the γ-Fe_2O_3-PR particles to Pd in Pd/γ-Fe_2O_3-PR as revealed by the XPS measurements, the activated dihydrogen or hydride on the Pd particles would get charge compensation from Pd. These hydrogen species with negative charge might prefer the nucleophilic attack on the carbon–chlorine bond in *p*-CNB rather than the electrophilic attack on the carbon–chlorine bond in *p*-CAN. This might be another cause of the complete suppression of *p*-CAN hydrogenolysis over Pd/γ-Fe_2O_3-PR.

4. Conclusion

The hydrodechlorination of *p*-CAN in the hydrogenation of *p*-CNB was completely suppressed and the selectivity of *p*-CAN of 99.2% was achieved over a prepared Pd/γ-Fe_2O_3-PR nanocomposite catalyst. Increasing the reaction hydrogen pressure from 0.1 to 4 MPa not only enhanced the *p*-CAN formation rate by 3.2 times but also obviously improved the *p*-CAN selectivity. Besides the hydrodechlorination of *p*-CNB, a new hydrodechlorination pathway was revealed in the hydrogenation of *p*-CNB over Pd/γ-Fe_2O_3-PR, i.e. through the hydrodechlorination of 4,4′-dichloroazobenzene intermediate. Pd/γ-Fe_2O_3-PR could be separated from the catalytic reaction system conveniently by an applied magnetic field and reused for several times without any loss of the catalytic selectivity to *p*-CAN. Although the average diameter of noble metal particles in Pd/γ-Fe_2O_3-PR (12.5 nm) is much larger than that in the previously

reported Pt/γ-Fe_2O_3-PR catalyst (2.2 nm), the catalytic activity for the reaction of interest at 303 K and 0.1 MPa over Pd/γ-Fe_2O_3-PR is higher than that over Pt/γ-Fe_2O_3-PR. XPS characterization revealed that an electron transfer occurred from the partially reduced γ-Fe_2O_3 particles to the Pd particles in Pd/γ-Fe_2O_3-PR. IR-CO and CO chemisorption measurements revealed that CO could hardly be chemisorbed on the Pd particles in Pd/γ-Fe_2O_3-PR under our experimental conditions. We believe that the electronic and adsorptive characteristics of Pd/γ-Fe_2O_3-PR are important causes of the superior selectivity to *p*-CAN in the hydrogenation of *p*-CNB over this catalyst.

Acknowledgements

This work is jointly supported by NSFC (20573005, 50821061, 90606017), NKBRSF (2006CB806102) from Chinese Ministry of Science and Technology, and RFDP of the Ministry of Education of China. We thank Dr. Yuexiang Zhu and Mr. Shuliang Lu at Peking University for the assistance in the CO chemisorption measurements.

Appendix A. Supplementary data

Supplementary data associated with this article can be found, in the online version, at doi:10.1016/j.molcata.2009.03.033.

References

[1] V. Krathy, M. Kralik, M. Mecarova, M. Stolcova, L. Zalibera, M. Hronec, Appl. Catal. A 235 (2002) 225.
[2] X.D. Wang, M.H. Liang, J.L. Zhang, Y. Wang, Curr. Org. Chem. 11 (2007) 299.
[3] F. Cardenas-Lizana, S. Gomez-Quero, M.A. Keane, Appl. Catal. A 334 (2008) 199.
[4] B. Coq, A. Tijani, F. Figueras, J. Mol. Catal. 68 (1991) 331.
[5] B. Coq, A. Tijani, R. Dutartre, F. Figueras, J. Mol. Catal. 79 (1993) 253.
[6] X.L. Yang, H.F. Liu, Appl. Catal. A 164 (1997) 197.
[7] W.Y. Yu, H.F. Liu, X.H. An, X.M. Ma, Z.J. Liu, L. Qiang, J. Mol. Catal. A 147 (1999) 73.
[8] X.X. Han, R.X. Zhou, X.M. Zheng, H. Jiang, J. Mol. Catal. A 193 (2003) 103.
[9] X.X. Han, R.X. Zhou, G.H. Lai, B.H. Yue, X.M. Zheng, J. Mol. Catal. A 209 (2004) 83.
[10] Y. Wang, J.W. Ren, K. Deng, L.L. Gui, Y.Q. Tang, Chem. Mater. 12 (2000) 1622.
[11] J.L. Zhang, Y. Wang, H. Ji, Y.G. Wei, N.Z. Wu, B.J. Zuo, Q.L. Wang, J. Catal. 229 (2005) 114.
[12] X.D. Wang, M.H. Liang, H.Q. Liu, Y. Wang, J. Mol. Catal. A 273 (2007) 160.
[13] M.H. Liang, X.D. Wang, H.Q. Liu, H.C. Liu, Y. Wang, J. Catal. 255 (2008) 335.
[14] J.R. Kosak, in: W.H. Jones (Ed.), Catalysis in Organic Syntheses, Academic Press, New York, 1980, p. 107.
[15] Z.K. Yu, S.J. Liao, Y. Xu, B. Yang, D.R. Yu, J. Chem. Soc., Chem. Commun. (1995) 1155.
[16] X.L. Yang, H.F. Liu, H. Zhong, J. Mol. Catal. A 147 (1999) 55.
[17] Q. Xu, X.M. Liu, J.R. Chen, R.X. Li, X.J. Li, J. Mol. Catal. A 260 (2006) 299.
[18] V. Vishwanathan, V. Jayasri, P.M. Basha, N. Mahata, L. Sikhwivhilu, N.J. Coville, Catal. Commun. 9 (2008) 453.
[19] Z.K. Yu, S.J. Liao, Y. Xu, B. Yang, D.R. Yu, J. Mol. Catal. A 120 (1997) 247.
[20] M.H. Liu, W.Y. Yu, H.F. Liu, J.M. Zheng, J. Colloid Interface Sci. 214 (1999) 231.
[21] W.X. Tu, S.J. Cao, L.P. Yang, W.C. Wang, Chem. Eng. J. 143 (2008) 244.
[22] P.N. Rylander, in: J.R. Anderson, M. Boudart (Eds.), Catalysis: Science and Technology, vol. 4, Akademie-Verlag, Berlin, 1993, p. 1.
[23] V.R. Chandrashekhar, R.V. Chaudhari, Ind. Eng. Chem. Res. 33 (1994) 1645.
[24] H. Arnold, F. Dobert, J. Gaube, in: G. Ertl, H. Knozinger, J. Weitkamp (Eds.), Handbook of Heterogeneous Catalysis, vol. 5, Wiley, New York, 1997, p. 2165.
[25] K. Weissermel, H.J. Arpe, Industrial Organic Chemistry, 3rd edition, VCH, Weinheim, 1997.
[26] C.Y. Xi, H.Y. Cheng, J.M. Hao, S.X. Cai, F.Y. Zhao, J. Mol. Catal. A 282 (2008) 80.
[27] L.M. Sikhwivhilu, N.J. Coville, B.M. Pulimaddi, J. Venkatreddy, V. Vishwanathan, Catal. Commun. 8 (2007) 1999.
[28] Powder Diffraction File Hanawalt Search Manual, Inorganic Phase, Sets, 1-42, International Centre for Diffraction Data, Pennsylvania, 1992.
[29] M. Descostes, F. Mercier, N. Thromat, C. Beaucaire, M. Gautier-Soyer, Appl. Surf. Sci. 165 (2000) 288.
[30] B.J. Zuo, Y. Wang, Q.L. Wang, J.L. Zhang, N.Z. Wu, L.D. Peng, L.L. Gui, X.D. Wang, R.M. Wang, D.P. Yu, J. Catal. 222 (2004) 493.
[31] Y. Lu, J.C. Liu, G. Diffee, D.S. Liu, B. Liu, Tetrahedron Lett. 47 (2006) 4597.
[32] A. Angeloff, J.J. Brunet, P. Legars, D. Neibecker, D. Souyri, Tetrahedron Lett. 42 (2001) 2301.
[33] E.A. Sales, J. Jove, M.J. Mendes, F. Bozon-Verduraz, J. Catal. 195 (2000) 88.
[34] N. Sheppard, T.T. Nguyen, in: R.J.H. Clark, R.E. Hester (Eds.), Advances in Infrared and Raman Spectroscopy, vol. 5, Wiley, New York, 1978, p. 67.
[35] K.I. Hadjiivanov, G.N. Vayssilov, Adv. Catal. 47 (2002) 307.
[36] Y. Wang, N. Toshima, J. Phys. Chem. B 101 (1997) 5301.
[37] C.M. Piqueras, I.O. Costilla, P.G. Belelli, N.J. Castellani, D.E. Damiani, Appl. Catal. A 347 (2008) 1.
[38] S. Abbet, E. Riedo, H. Brune, U. Heiz, A.M. Ferrari, L. Giordano, G. Pacchioni, J. Am. Chem. Soc. 123 (2001) 6172.
[39] T. Yoneda, T. Takido, K. Konuma, J. Mol. Catal. A 265 (2007) 80.